

Constraints on the Early and Late Integrated Sachs-Wolfe effects from Planck 2015 Cosmic Microwave Background Anisotropies angular power spectra

Giovanni Cabass,¹ Martina Gerbino,¹ Elena Giusarma,¹ Alessandro Melchiorri,¹ Luca Pagano,¹ and Laura Salvati¹

¹*Physics Department and INFN, Università di Roma “La Sapienza”, P.le Aldo Moro 2, 00185, Rome, Italy*

The Integrated Sachs-Wolfe (ISW) effect predicts additional anisotropies in the Cosmic Microwave Background due to time variation of the gravitational potential when the expansion of the universe is not matter dominated. The ISW effect is therefore expected in the early universe, due to the presence of relativistic particles at recombination, and in the late universe, when dark energy starts to dominate the expansion. Deviations from the standard picture can be parameterized by $A_{e\text{ISW}}$ and $A_{l\text{ISW}}$, which rescale the overall amplitude of the early and late ISW effects. Analyzing the most recent CMB temperature spectra from the Planck 2015 release, we detect the presence of the early ISW at high significance with $A_{e\text{ISW}} = 1.06 \pm 0.04$ at 68% CL and an upper limit for the late ISW of $A_{l\text{ISW}} < 1.1$ at 95% CL. The inclusion of the recent polarization data from the Planck experiment results in $A_{e\text{ISW}} = 0.999 \pm 0.028$ at 68% CL, in better agreement with the value $A_{e\text{ISW}} = 1$ of a standard cosmology. When considering the recent detections of the late ISW coming from correlations between CMB temperature anisotropies and weak lensing, a value of $A_{l\text{ISW}} = 0.85 \pm 0.21$ is predicted at 68% CL, showing a 4σ evidence. We discuss the stability of our result in the case of an extra relativistic energy component parametrized by the effective neutrino number N_{eff} and of a CMB lensing amplitude A_L .

PACS numbers: 98.80.Es, 98.80.Jk, 95.30.Sf

I. INTRODUCTION

Already in 1966, only two years after the discovery of the Cosmic Microwave Background (hereafter, CMB) radiation [1], R. K. Sachs and A. M. Wolfe presented the first computations of the gravitational redshift of CMB photons by linear matter perturbations [2]. This so called “Sachs-Wolfe” (SW) effect can be identified in two regimes: the Non-Integrated SW (NISW) effect and the Integrated SW effect (ISW). The NISW is the predominant source of fluctuations in the CMB on scales larger than ~ 10 degrees. This effect, measured for the first time by the COBE satellite in 1992 [3], occurs at the last scattering surface and provides the first indication for a nearly scale invariant spectrum of primordial fluctuations, as expected in inflationary theory (see e.g. [4, 5]).

The ISW, on the contrary, is a “secondary” source of CMB fluctuations, always subdominant with respect to primary sources: it is produced between the last scattering surface and today, and it gives a non-zero contribution only if the expansion of the universe is not entirely driven by a non-relativistic matter component. Therefore it will be present after CMB decoupling (produced by the non-negligible relativistic energy component in the total energy density – early ISW), and at recent times when the expansion of the Universe starts to be affected by dark energy (late ISW).

Both $e\text{ISW}$ and $l\text{ISW}$ provide an excellent probe for “new physics”. A measurement of a late ISW is indeed an evidence for a non-dark matter dominated expansion of the late Universe, confirming the existence of a “dark energy” component. The $l\text{ISW}$, combined with other cosmological observables, could also be used to constrain dark energy parameters as its equation of state or effective sound speed (see e.g. [6–8]). Moreover, the

use of the $l\text{ISW}$ to constrain the neutrino mass has been proposed by [9].

The $e\text{ISW}$, on the contrary, probes the amount of energy stored in relativistic degrees of freedom at recombination. The presence of extra-light particles like sterile neutrinos or thermal axions at such epoch, then, can change its amplitude. The early ISW can also be used to constrain modified gravity models as discussed, for example, in [10].

The $l\text{ISW}$ has been detected for the first time in [11], by cross-correlating the map of the CMB sky measured by the WMAP satellite with number counts of radio galaxies in the NVSS survey and with the hard X-ray background measured by the HEAO-1 satellite.

This detection has then been confirmed several times in the past years by cross-correlations with different datasets [12–20]. The last analysis obtained by the Planck collaboration [21] found a $\sim 4\sigma$ indication for $l\text{ISW}$, with an amplitude in agreement with a cosmological constant making up the entirety of the dark energy component.

The $e\text{ISW}$ cannot be probed directly, but it affects the CMB angular spectrum of temperature anisotropies (see e.g. [22] and the discussion in the next Section). Constraints on the amplitude of the $e\text{ISW}$ coming from the WMAP satellite have been presented in [22].

In this paper we present new constraints on the $l\text{ISW}$ and the $e\text{ISW}$ effects from the recent measurements of the CMB temperature and polarization angular power spectrum provided by the Planck satellite, and also discuss degeneracies with other parameters. Most notably, we found a correlation between the amplitude of the $e\text{ISW}$ and the effective lensing parameter A_L in discrepancy with the standard value at about ~ 2 standard deviations.

The paper is organized as follows: in the next Section we describe the physics of the ISW effect and the parametrization we have used. In Section III we present our data analysis method, in Section IV we discuss our results and, finally, in Section V we derive our conclusions.

II. THE ISW EFFECT

The Integrated Sachs-Wolfe (ISW) effect is a contribution to the CMB temperature anisotropy given by the interaction of photons with time-dependent gravitational potentials. At multipole ℓ and linear order in temperature perturbations one has that [23]

$$\Theta_\ell^{\text{ISW}}(k) = \int_0^{\eta_0} d\eta e^{-\tau(\eta)} \{ \dot{\Psi}(k, \eta) - \dot{\Phi}(k, \eta) \} j_\ell(k\Delta\eta), \quad (1)$$

where τ is the optical depth, η_0 is the current conformal time and $\Delta\eta \equiv \eta_0 - \eta$. For times much earlier than recombination ($\eta \ll \eta_{\text{rec}}$), CMB photons are tightly coupled to electrons and protons by Compton scattering: this makes $e^{-\tau(\eta)}$ small enough that the ISW effect is negligible.

A. Early ISW – theory

Eq. (1) shows how there is a non-vanishing ISW effect in presence of time dependent gravitational potentials Ψ and Φ . For modes that cross the horizon well into matter domination, the gravitational potentials are constant in time. So one expects the ISW to be mainly present at times after recombination (since the energy density of relativistic matter is still considerable at that time). Because of this, one can estimate its contribution to multipole ℓ by evaluating the Bessel function at $\eta \sim \eta_{\text{rec}}$: the result is (approximating $\Phi \approx -\Psi$)

$$\Theta_\ell^{e\text{ISW}}(k) \approx 2j_\ell(k\Delta\eta_{\text{rec}}) \{ \Psi(k, \eta_{\text{MD}}) - \Psi(k, \eta_{\text{rec}}) \}, \quad (2)$$

where η_{MD} is a time late at matter domination. From Eq. (2) one can see that [24]:

- the early ISW adds in phase with the Sachs-Wolfe primary anisotropy, given by

$$\Theta_\ell^{\text{SW}}(k) = j_\ell(k\Delta\eta_{\text{rec}}) \{ \Theta_0(k, \eta_{\text{rec}}) + \Psi(k, \eta_{\text{rec}}) \}. \quad (3)$$

We can see this from the fact that both anisotropies are multiplied by the same Bessel function. This will increase the height of the first acoustic peaks, with the first one being boosted more than the others. The reason is that at times right after recombination, perturbations with $k \ll 1/\eta_{\text{rec}}$ do not evolve, while perturbations with $k \gg 1/\eta_{\text{rec}}$ are averaged out when integrated along the photon trajectory. This means that the dominant contribution to the early ISW effect is due to perturbations with $k \sim 1/\eta_{\text{rec}}$, that approximately corresponds to the first acoustic peak;

- the effect of $\Theta_\ell^{e\text{ISW}}(k)$ on the angular anisotropy C_ℓ is suppressed by the factor

$$\frac{\rho_{\text{rad}}^2(\eta_{\text{rec}})}{\rho_{\text{m}}^2(\eta_{\text{rec}})} = \left(\frac{1 + z_{\text{rec}}}{1 + z_{\text{eq}}} \right)^2. \quad (4)$$

Therefore, even if neutrinos and other relativistic species decoupled from the primordial plasma earlier than the photons, the ISW will still depend on the number of relativistic degrees of freedom at recombination: an increase of the amount of radiation during this epoch (i.e. an effective number of relativistic species $N_{\text{eff}} > 3.046$) will delay the advent of matter domination, make z_{eq} smaller, and result in a larger amplitude of the early ISW effect.

This is one of the main reasons why the Cosmic Microwave Background is sensitive to the redshift of matter-radiation equality (and then to the amount of radiation at recombination), thus opening the possibility of constraining the number of extra relativistic species with CMB experiments.

B. Late ISW – theory

The late ISW effect is active at more recent times, when dark energy starts to play a role and the gravitational potentials are decreasing, and its contribution to the CMB power spectrum is sizable at large scales only [25]. The observable effects of the ISW, in the times dominated by dark energy, are mainly the following [26]:

- focusing on scales corresponding to galaxy clusters, where gravitational perturbations start growing, the CMB photons experience an ISW effect caused by the time-dependence of the gravitational potential inside these non-linear structures. Therefore one expects to find a correlation between C_ℓ^{ISW} and the density contrast observed by surveys [27, 28]. These correlations can be used to distinguish between the standard Λ CDM universe and models that try to explain the present day acceleration through modifications of gravity [32, 33];
- the gravitational potentials that redshift CMB photons (late ISW) are the same that cause the weak lensing distortions: the interplay between these two effects gives rise to a non-Gaussian contribution, which is encoded in the lensing-induced bispectrum between small and large angular scales [29].

The correlation with these LSS tracers has been investigated in [21], which studied the cross-correlations of the temperature anisotropies with both lensing potential and galaxy number counts, showing that they yield a 4σ detection of the late ISW. More precisely, temperature-lensing correlations result in $A_{\text{ISW}} = 1.04 \pm 0.33$, while including galaxy number counts gives $A_{\text{ISW}} = 1.00 \pm 0.25$.

C. Parametrization of early and late ISW effects

In this paper we consider a parametrization of the ISW amplitude in terms of two parameters $A_{e\text{ISW}}$ and $A_{l\text{ISW}}$, which rescale the contribution at early ($A_{e\text{ISW}}$) and late ($A_{l\text{ISW}}$) times in the following way: we introduce in the integrand of Eq. (1) a function $f(\eta)$ given by

$$f(\eta) = \begin{cases} A_{e\text{ISW}} & \text{for } z > 30, \\ A_{l\text{ISW}} & \text{for } z < 30, \end{cases} \quad (5)$$

where the standard scenario is given by $A_{e\text{ISW}} = A_{l\text{ISW}} = 1$. The reason why we have chosen $z = 30$ as a turning point between the early and late contributions is merely a phenomenological one: plotting the integrand of Eq. (1) as a function of redshift with the `camb` code [34], one can see that its minimum lies near $z = 30$.

III. DATA ANALYSIS METHOD

We perform a Markov-chain Monte-Carlo (MCMC) analysis, making use of the publicly available code `cosmomc` [35, 36]. Our baseline model is the standard six-parameter ΛCDM model, which includes the baryon density $\Omega_b h^2$, the cold dark matter density $\Omega_c h^2$, the sound horizon angular scale θ , the reionization optical depth τ , the amplitude and spectral index of the primordial power spectrum of scalar perturbations $\ln[10^{10} A_s]$ and n_s . We then include the two amplitudes $A_{e\text{ISW}}$ and $A_{l\text{ISW}}$ of Eq. (5).

We firstly fix one of the two amplitudes to the standard expected value and let the second one to vary freely, but also explore the case of the two amplitudes varying jointly. In addition, we consider other one-parameter extensions to this $\Lambda\text{CDM} + A_{\text{ISW}}$ model, by varying separately the gravitational lensing amplitude A_L [37], the primordial helium abundance Y_P (assuming it to be an independent parameter in a non-standard BBN framework) and T_{CMB} (the blackbody temperature of the CMB at the current epoch). When not varied, these parameters are fixed in agreement with the standard cosmological scenario, namely:

- $A_L = 1$;
- $N_{\text{eff}} = 3.046$;
- Y_P as a function of $\Omega_b h^2$ and the effective number of relativistic species N_{eff} equal to 3.046 (as expected from the standard BBN);
- $T_0 = 2.7255 \text{ K}$ [38].

We impose flat priors, but also check the impact of a gaussian prior $A_{l\text{ISW}} = 1.00 \pm 0.25$ (which will be denoted by the “prior” label in the following plots and tables). This prior is consistent with the 68% CL bounds on the same parameter from [21], where the ISW-lensing

bispectrum induced on the Gaussian CMB anisotropies by the lensing effect is estimated by cross-correlating the Planck CMB maps with the Planck map of the lensing potential [21].

We test the following datasets: the high- ℓ Planck temperature and polarization power spectra in the range $30 \leq \ell < 2500$ (hereafter *Planck* TT and *Planck* TE, EE) combined with the low- ℓ Planck temperature and polarization power spectra in the range $2 \leq \ell < 29$ (denoted as lowP) [39]. Regarding polarization spectra at high ℓ , we also test the WMAP power spectra in temperature and polarization [40] up to $\ell = 1200$. When T_0 is varied, we also add information from baryon acoustic oscillation (BAO) as reported in [41], in order to break degeneracies among cosmological parameters.

IV. RESULTS

A. Early ISW – results

We start from considering the case in which only the early ISW effect is left free to vary. The results of our analysis are shown in Tabs. I and II in which we report the 68% CL around the mean value of the posterior.

By comparing the results given in the first column of Table I with those shown by the Planck Collaboration in [41] for a ΛCDM model, it can be noticed that the most interesting effects which arise from the inclusion of $A_{e\text{ISW}}$ as a free parameter are on the parameters $\Omega_b h^2$ and n_s : a lower $\Omega_b h^2$ and a higher n_s than the standard ΛCDM case are favored.

This can be understood looking at Fig. 1, which shows the correlation between $A_{e\text{ISW}}$ with $\Omega_b h^2$ and n_s . A larger $A_{e\text{ISW}}$ or a larger $\Omega_b h^2$ act in (almost) the same way on the CMB spectrum, increasing the height of the peaks at $\ell \sim 100$. This is reflected in the strong degeneracy between $A_{e\text{ISW}}$ and $\Omega_b h^2$ (left panel of Fig. 1), in fact a higher value of $A_{e\text{ISW}}$ can be compensated by a decrease of $\Omega_b h^2$ to keep fixed the height of the acoustic peaks of the CMB. The right panel of Fig. 1 shows the the 68% CL and 95% CL allowed regions in the $(n_s, A_{e\text{ISW}})$ plane: as the value of n_s increases, a larger $A_{e\text{ISW}}$ is also allowed.

When we consider the *Planck* TT,TE,EE+lowP datasets (first column of Table II) the bounds on the optical depth, τ , and on the amplitude of the primordial spectrum, $\ln[10^{10} A_s]$, are displaced to higher values and the errors on the cosmological parameters are reduced.

Instead, as shown in Tables I and II, the inclusion of gravitational lensing, A_L , and of the effective number of relativistic species, N_{eff} , does not change significantly the constraints on the parameters with respect to those obtained by the Planck Collaboration [41]. Figure 2, left panel, depicts the 68% and 95% CL allowed regions in the $(A_L, A_{e\text{ISW}})$ plane. Even if the early ISW and weak lensing operate at very different scales, the latter is also sensitive to the matter density $\Omega_m h^2$ [42]: this explains

TABLE I. Constraints at 68% CL on the cosmological parameters in the extended Λ CDM model explored here using the *Planck* TT+lowP dataset.

Parameter	Λ CDM + $A_{e\text{ISW}}$	Λ CDM + N_{eff} + $A_{e\text{ISW}}$	Λ CDM + A_L + $A_{e\text{ISW}}$
$\Omega_b h^2$	0.0218 ± 0.0004	0.0218 ± 0.0005	0.0225 ± 0.0005
$\Omega_c h^2$	0.1201 ± 0.0022	0.1204 ± 0.0039	0.1170 ± 0.0027
100θ	1.04072 ± 0.00049	1.04071 ± 0.00056	1.04126 ± 0.00056
τ	0.076 ± 0.019	0.077 ± 0.022	0.059 ± 0.020
n_s	0.9724 ± 0.0080	0.974 ± 0.016	0.9750 ± 0.0081
$\ln[10^{10} A_s]$	3.080 ± 0.037	3.083 ± 0.048	3.045 ± 0.041
N_{eff}	$\equiv 1$	$3.08^{+0.29}_{-0.34}$	$\equiv 3.046$
A_L	$\equiv 1$	$\equiv 1$	1.216 ± 0.11
$A_{e\text{ISW}}$	$1.064^{+0.042}_{-0.043}$	1.065 ± 0.043	1.018 ± 0.046

TABLE II. Constraints at 68% CL on extensions of the Λ CDM model for the *Planck* TT,TE,EE+lowP dataset.

Parameter	Λ CDM + $A_{e\text{ISW}}$	Λ CDM + N_{eff} + $A_{e\text{ISW}}$	Λ CDM + A_L + $A_{e\text{ISW}}$
$\Omega_b h^2$	0.0222 ± 0.0002	0.0222 ± 0.0003	0.0225 ± 0.0002
$\Omega_c h^2$	0.1199 ± 0.0015	0.1189 ± 0.0031	$0.1183^{+0.0016}_{-0.0015}$
100θ	1.04072 ± 0.00031	1.04087 ± 0.00045	1.04095 ± 0.00032
τ	0.081 ± 0.017	0.080 ± 0.018	$0.056^{+0.021}_{-0.020}$
n_s	0.9638 ± 0.0058	0.961 ± 0.010	0.967 ± 0.0055
$\ln[10^{10} A_s]$	3.098 ± 0.033	3.091 ± 0.038	$3.042^{+0.043}_{-0.040}$
N_{eff}	$\equiv 1$	$2.99^{+0.20}_{-0.21}$	$\equiv 3.046$
A_L	$\equiv 1$	$\equiv 1$	$1.182^{+0.076}_{-0.086}$
$A_{e\text{ISW}}$	0.999 ± 0.028	1.002 ± 0.028	0.988 ± 0.027

the mild correlation between these two parameters shown in the left panel. The right panel of Figure 2 illustrates the 68% and 95% CL contours in the $(N_{\text{eff}}, A_{e\text{ISW}})$ plane resulting from the analysis of CMB data. Notice that, in contrast to what said in section II A, these parameters appear uncorrelated. Actually, instead, this agrees with the conclusions of [43], in which the authors explain how a Y_P “fixed” by BBN consistency would not degrade the constraint on N_{eff} , even if $A_{e\text{ISW}}$ is left free to vary.

Tab. III depicts the 68% CL constraints on $A_{e\text{ISW}}$ for the different cosmological models explored in this study using different cosmological data. Firstly, notice that the *Planck* TT+lowP data alone already provide tighter constraints than WMAP on $A_{e\text{ISW}}$. Using only the *Planck* TT+lowP data, we can see that the inclusion of the lensing amplitude A_L as a free parameter (in addition to the standard Λ CDM picture) tends to diminish the 1σ indication for a $A_{e\text{ISW}} \neq 1$. We also note that this preference persists when we vary other parameters like the effective

number of relativistic species N_{eff} , the running of the scalar tilt n_{run} and the Helium mass fraction Y_P . On the other hand, it vanishes when we consider the *Planck* TT,TE,EE+lowP data for all different cosmological models. These results are also summarized by the plots of Fig. 3, showing the one-dimensional posteriors for $A_{e\text{ISW}}$ in the various extensions of Λ CDM we discussed.

Figure 4 shows the 2D marginalized posterior distribution for $\Omega_b h^2$ and n_s using the *Planck* TT+lowP and *Planck* TT,TE,EE+lowP datasets. We consider two different cosmological models: Λ CDM vs. Λ CDM+ $A_{e\text{ISW}}$. Notice that the correlation between $\Omega_b h^2$ and n_s turns from positive (Λ CDM) to negative (Λ CDM + $A_{e\text{ISW}}$). This is due to the strong degeneracy between $\Omega_b h^2$ and $A_{e\text{ISW}}$ (already shown in Fig. 1) that reduces the degeneracies between the other parameters of the Λ CDM model. Moreover, if also the information from the *Planck* high- ℓ polarization data is included, the values of these three parameters tend to come in accord with their stan-

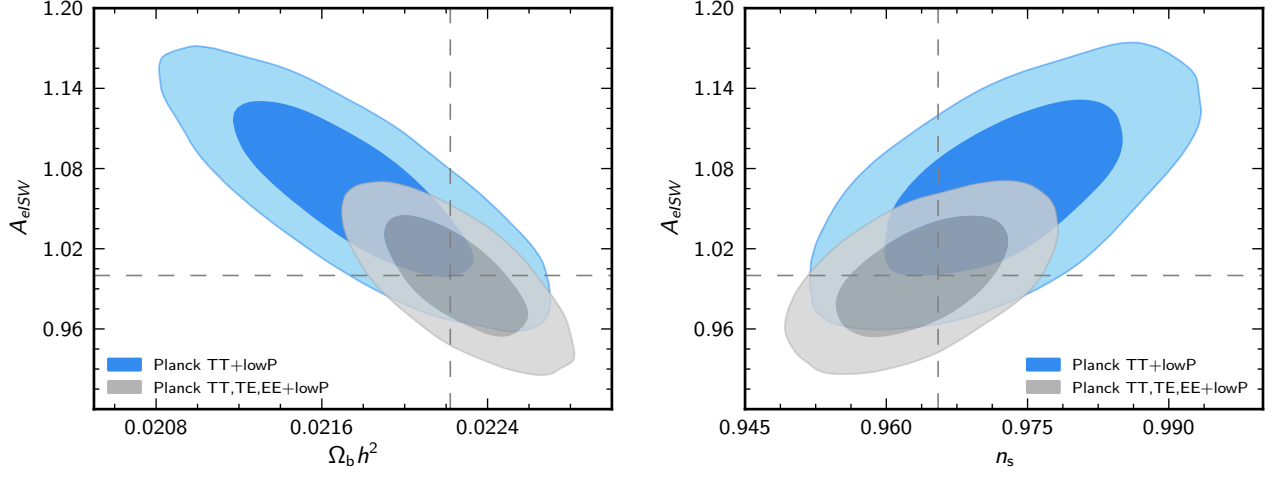


FIG. 1. Two-dimensional posterior probability in the $(\Omega_b h^2, A_{e\text{ISW}})$ and $(n_s, A_{e\text{ISW}})$ planes for the *Planck* TT+lowP dataset and the *Planck* TT,TE,EE+lowP datasets.

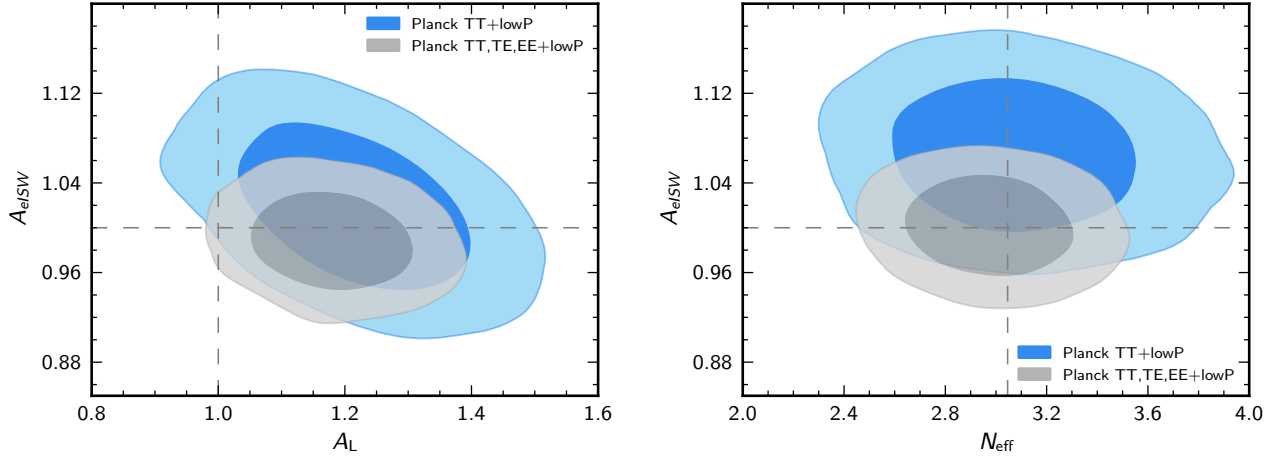


FIG. 2. The left panel depicts the 68% and 95% CL allowed regions in the $(A_L, A_{e\text{ISW}})$ plane for the *Planck* TT+lowP and the *Planck* TT,TE,EE+lowP datasets. The right panel shows the 68% and 95% CL regions in the $(N_{\text{eff}}, A_{e\text{ISW}})$ plane.

dard Λ CDM value (see Tab. III), even if the direction of the degeneracy between $\Omega_b h^2$ and n_s remains positive.

B. Late ISW – results

In this section we present the results obtained considering only the late ISW effect. Table IV presents the constraints on A_{IISW} for the different cosmological data combinations considered here. Fig. 5 contains the one-dimensional posteriors for the amplitude of the late-time ISW effect in the various extensions of Λ CDM model. Notice that when we consider the case with a flat prior on A_{IISW} , there is consistency with $A_{\text{IISW}} = 1$ for the WMAP dataset. The *Planck* TT+lowP and the *Planck*

TT, TE, EE+lowP measurements set the 95% CL upper limit of $A_{\text{IISW}} \lesssim 1.14$ and $A_{\text{IISW}} \lesssim 1.11$ respectively. We note that Planck alone does not improve significantly the constraint on A_{IISW} with respect to WMAP measurements. This occurs because the late-time ISW affects a region of CMB power spectrum multipoles that is dominated by cosmic variance, rather than by instrumental precision. Moreover the bounds on A_{IISW} are not affected if the effective number of relativistic species (N_{eff}) is included.

We also consider a gaussian prior of $A_{\text{IISW}} = 1.00 \pm 0.25$ from the bispectrum-LSS cross-correlation analysis, which allows us to take into account the constraints on the late ISW coming from large-scale structure measurements. The inclusion of the prior results in a tighter

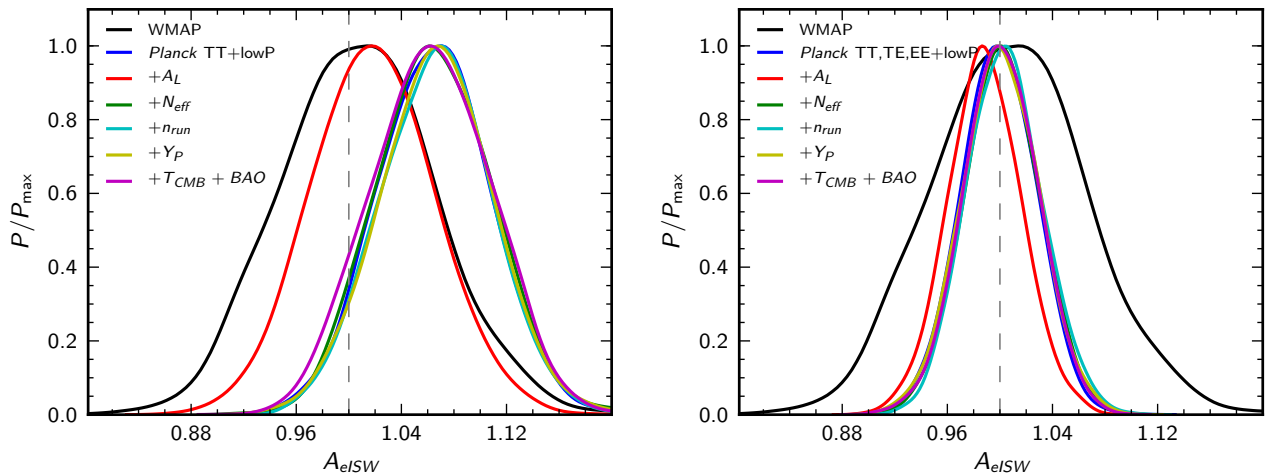


FIG. 3. One-dimensional posterior probability for the amplitude of the early-time ISW effect for the indicated datasets and models. The black and blue curves correspond to a Λ CDM + $A_{e\text{ISW}}$ model. The additional curves come from the indicated one-parameter extension to this baseline model, for the *Planck* TT+lowP dataset (left) and *Planck* TT,TE,EE+lowP dataset (right). When T_{CMB} is varied, BAO datasets [44–48] are included in the analysis, in order to break degeneracies between cosmological parameters.

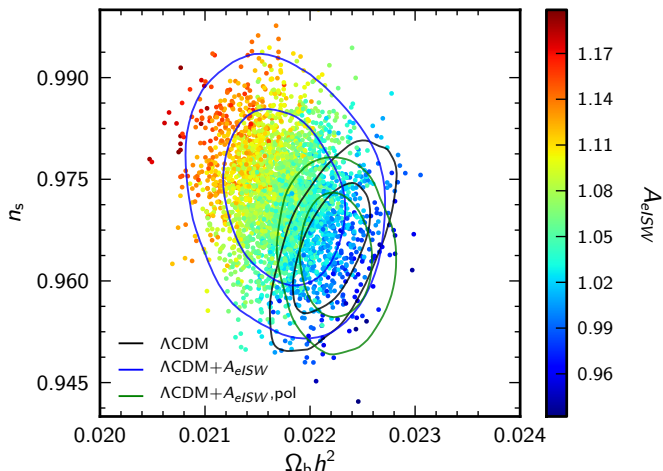


FIG. 4. Two-dimensional contours in the $\Omega_b h^2 - n_s$ plane, colored by the value of the parameter $A_{e\text{ISW}}$, for the *Planck* TT+lowP and *Planck* TT,TE,EE+lowP datasets. The black and blue contours show the two-dimensional posterior probability in the $\Omega_b h^2 - n_s$ plane for the same dataset and the indicated models. The green contours include the addition of high- ℓ polarization.

constraints from WMAP, while the posterior on A_{ISW} when Planck data set is considered is shifted towards $A_{\text{ISW}} = 1$.

Fig. 6 shows the 68% and 95% CL allowed regions in the (A_L, A_{ISW}) plane for the *Planck* TT+lowP and *Planck* TT,TE,EE+lowP data sets. Notice that there is no correlation between $A_L - A_{\text{ISW}}$. This was expected

since the late ISW is active at low ℓ , while weak lensing operates at high ℓ . Moreover there is a mild preference for a non-standard value of both parameters. Marginalizing over A_L we obtain an upper limit of $A_{\text{ISW}} < 1.25$ at 95% CL using the *Planck* TT+lowP data set, while the inclusion of high- ℓ polarization measurements tightens the constraint at $A_{\text{ISW}} < 1.12$ at 95% CL.

C. Early + late ISW

We conclude by considering the case of both $A_{e\text{ISW}}$ and A_{ISW} varying jointly. Constraints on these two parameters are reported in Tab. V. The one-dimensional and two-dimensional posterior probabilities for a selected subset of datasets and models are shown in Fig. 7. As mentioned in Sec. IV A and IV B, when compared with the results from WMAP, the Planck data provide much tighter constraints on $A_{e\text{ISW}}$ even when considering temperature only, while the constraining power on A_{ISW} is comparable.

The upper bounds on A_{ISW} are well compatible with the standard case for all datasets used, while there is a 1σ preference of $A_{e\text{ISW}} \neq 1$ when using the *Planck* TT+lowP dataset. We note, though, that such a preference for $A_{e\text{ISW}} \neq 1$ disappears when we let A_L free to vary, as a result of the mild degeneracy between the two parameters discussed in Sec. IV A. Allowing the number of relativistic species to vary does not alter the constraints with respect to the minimal extension to Λ CDM.

The inclusion of small-scale polarization data significantly tightens the constraints on $A_{e\text{ISW}}$, almost halving the posterior width. On the other hand, as already ex-

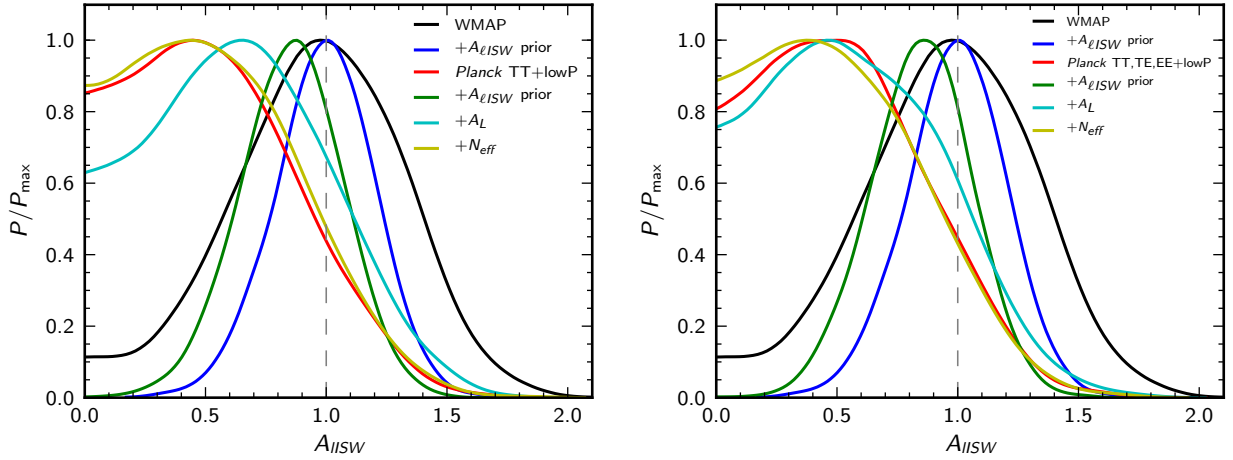


FIG. 5. One-dimensional posterior probability for the amplitude of the late-time ISW effect for the data sets and models discussed in the text. The black curves refer to a Λ CDM + A_{lISW} , with the WMAP data set for the high- ℓ polarization. The remaining curves include the *Planck* TT+lowP data (left panel), and the *Planck* TT,TE,EE+lowP data (right panel). The “ A_{lISW} prior” label indicates the inclusion of the gaussian prior on A_{lISW} coming from the cross-correlated analysis of the CMB bispectrum and galaxy clusters.

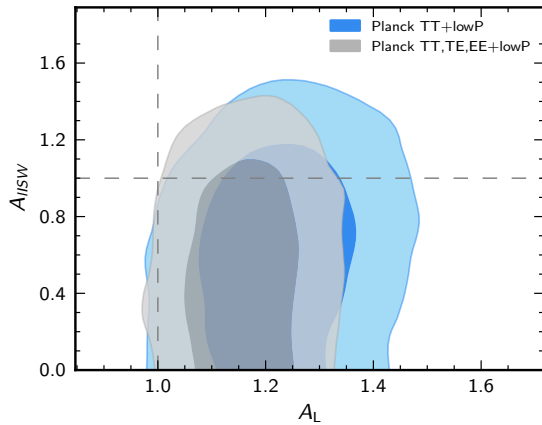


FIG. 6. Two-dimensional posterior probability in the $A_L - A_{lISW}$ plane for the *Planck* TT+lowP and *Planck* TT,TE,EE+lowP datasets. This posterior shows that, while the amplitude of the late ISW effect and the lensing parameter A_L are not correlated, the inclusion of high- ℓ polarization data from Planck brings the contours back in accord with $A_L = 1$ and $A_{lISW} = 1$.

pected, it does not provide further information on A_{lISW} , as highlighted by the superposition of both the green curves with the solid red one in the top right panel of Fig. 7.

V. CONCLUSIONS

In this paper we study the constraints on the amplitude of the Integrated Sachs Wolfe effect, both its early and

late time contributions.

We find that the *Planck* TT+lowP data is consistent with a non-zero early ISW, with an amplitude A_{eISW} in agreement with $A_{eISW} = 1$ as predicted by theory, with a 1σ preference of $A_{eISW} \neq 1$ when considering extensions to the Λ CDM model discussed in this work. We also confirm the strong degeneracy between the amplitude of the early ISW and parameters like $\Omega_b h^2$ and n_s . Our analysis also hints for a correlation between A_{eISW} and the lensing parameter A_L .

Regarding the late ISW, Planck data alone place a constraint $A_{lISW} \lesssim 1.1$ at 95% CL. When supplemented with a prior on A_{lISW} coming from CMB temperature anisotropies-weak lensing correlations, however, we find a $\sim 4\sigma$ detection $A_{lISW} = 0.85 \pm 0.21$.

When we consider also the recent polarization data at high ℓ from the Planck collaboration, we find that the evidences for a non-standard value of A_{eISW} disappear. The reason is that the addition of *TE* and *EE* spectra leads to a better agreement of data with the standard Λ CDM model. More precisely, A_{eISW} gets dragged towards 1 through its degeneracy with $\Omega_b h^2$ and n_s , which return in agreement with the Λ CDM best fit when polarization is included.

On the other hand, using the small-scale polarization spectra does not change the results obtained for A_{lISW} . Their effect is to slightly tighten the upper bounds obtained when considering only the temperature spectra.

When the two parameters are allowed to vary jointly, the same pattern described above is reproduced.

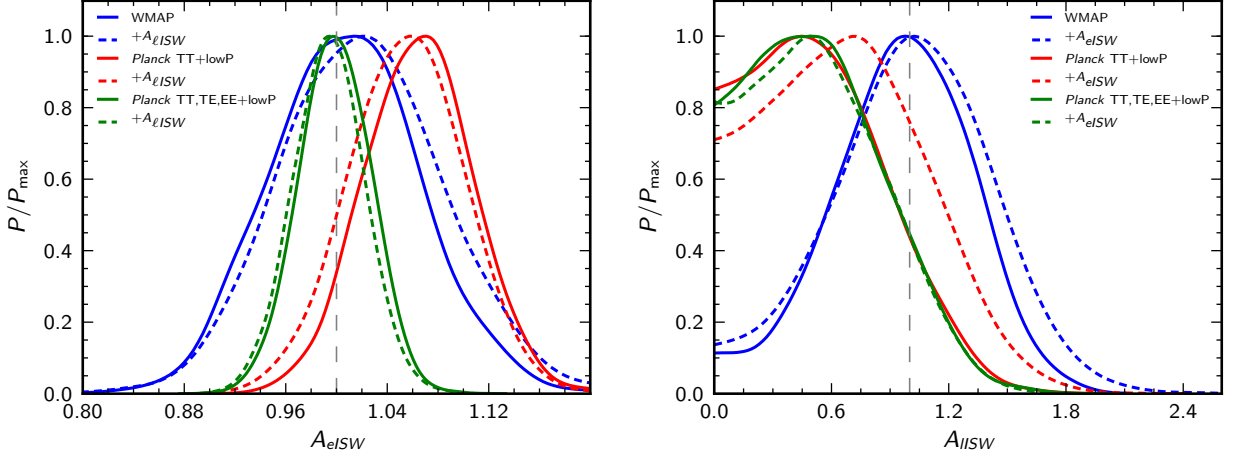


FIG. 7. One-dimensional posterior probability for the amplitude of the early-time ISW effect (left) and late-time ISW effect (right) for the indicated datasets and models. For each plot, the solid curves have been obtained for the corresponding one-parameter extension to the base Λ CDM model. The dashed curves correspond to the joint variation of A_{eISW} and A_{lISW} .

Extended Model Λ CDM+	A_{eISW}
A_{eISW}	
WMAP	$1.007^{+0.056}_{-0.058}$
<i>Planck</i> TT+lowP	$1.064^{+0.042}_{-0.043}$
<i>Planck</i> TT, TE, EE+lowP	0.999 ± 0.028
$A_{eISW} + A_L$	
<i>Planck</i> TT+lowP	1.018 ± 0.046
<i>Planck</i> TT, TE, EE+lowP	0.988 ± 0.027
$A_{eISW} + N_{eff}$	
<i>Planck</i> TT+lowP	1.065 ± 0.043
<i>Planck</i> TT, TE, EE+lowP	1.002 ± 0.028
$A_{eISW} + n_{run}$	
<i>Planck</i> TT+lowP	$1.066^{+0.041}_{-0.042}$
<i>Planck</i> TT, TE, EE +lowP	$1.004^{+0.027}_{-0.031}$
$A_{eISW} + Y_P$	
<i>Planck</i> TT+lowP	1.066 ± 0.042
<i>Planck</i> TT, TE, EE +lowP	1.000 ± 0.028
$A_{eISW} + T_{CMB}$	
<i>Planck</i> TT+lowP+BAO	1.063 ± 0.046
<i>Planck</i> TT, TE, EE +lowP+ BAO	1.001 ± 0.028

TABLE III. Constraints at 68% CL on the amplitude of the early-time ISW effect, A_{eISW} , for the different combinations of datasets and models.

Extended Model Λ CDM+	A_{lISW}
A_{lISW}	
WMAP	$0.958^{+0.391}_{-0.317}$
<i>Planck</i> TT+lowP	< 1.14 (95% CL)
<i>Planck</i> TT, TE, EE+lowP	< 1.11 (95% CL)
A_{lISW} , prior	
WMAP	$0.958^{+0.220}_{-0.192}$
<i>Planck</i> TT+lowP	0.853 ± 0.211
<i>Planck</i> TT, TE, EE+lowP	$0.847^{+0.217}_{-0.203}$
$A_{lISW} + N_{eff}$	
<i>Planck</i> TT+lowP	< 1.14 (95% CL)
<i>Planck</i> TT, TE, EE+lowP	< 1.11 (95% CL)
$A_{lISW} + A_L$	
<i>Planck</i> TT+lowP	< 1.25 (95% CL)
<i>Planck</i> TT, TE, EE +lowP	< 1.12 (95% CL)

TABLE IV. Constraints at 68% CL (unless otherwise stated) on the amplitude of the late-time ISW effect, A_{lISW} , for the different combinations of data sets and models considered in the text.

Acknowledgements

We would like to thank Antony Lewis for the use of the numerical codes `cosmomc` and `camb`. We acknowledge support by the research grant Theoretical Astroparticle

TABLE V. Constraints at 68% CL (unless otherwise stated) on the amplitude of the late-time ISW effect A_{ISW} and of the early-time ISW effect A_{eISW} for the indicated datasets and models.

Dataset, model	A_{ISW}	A_{eISW}
WMAP, $\Lambda\text{CDM} + A_{\text{ISW}} + A_{\text{eISW}}$	$1.011^{+0.434}_{-0.374}$	$1.019^{+0.061}_{-0.066}$
Planck <i>Planck</i> TT+lowP, $\Lambda\text{CDM} + A_{\text{ISW}} + A_{\text{eISW}}$	< 1.34 (95% CL)	1.055 ± 0.044
Planck <i>Planck</i> TT+lowP, $\Lambda\text{CDM} + A_{\text{ISW}} + A_{\text{eISW}} + A_{\text{L}}$	< 1.32 (95% CL)	$1.009^{+0.047}_{-0.048}$
Planck <i>Planck</i> TT+lowP, $\Lambda\text{CDM} + A_{\text{ISW}} + A_{\text{eISW}} + N_{\text{eff}}$	< 1.35 (95% CL)	$1.057^{+0.043}_{-0.044}$
Planck <i>Planck</i> TT,TE,EE+lowP, $\Lambda\text{CDM} + A_{\text{ISW}} + A_{\text{eISW}}$	< 1.11 (95% CL)	$0.994^{+0.027}_{-0.028}$
Planck <i>Planck</i> TT,TE,EE+lowP, $\Lambda\text{CDM} + A_{\text{ISW}} + A_{\text{eISW}} + A_{\text{L}}$	< 1.12 (95% CL)	0.985 ± 0.028
Planck <i>Planck</i> TT,TE,EE+lowP, $\Lambda\text{CDM} + A_{\text{ISW}} + A_{\text{eISW}} + N_{\text{eff}}$	< 1.10 (95% CL)	$0.996^{+0.028}_{-0.030}$

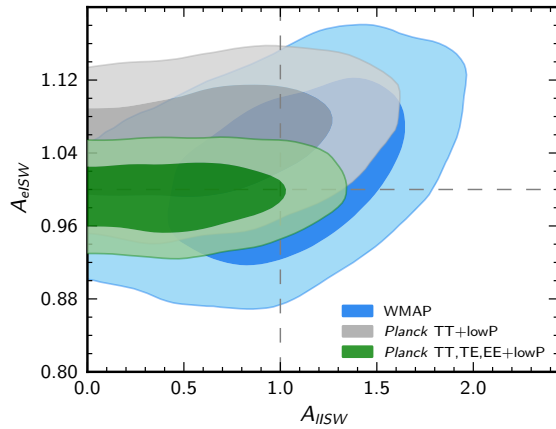


FIG. 8. Two-dimensional posterior probability in the $A_{\text{ISW}} - A_{\text{eISW}}$ plane for the *Planck* TT+lowP and *Planck* TT,TE,EE+lowP datasets.

Physics number 2012CPPYP7 under the program PRIN 2012 funded by MIUR and by TASP, iniziativa specifica INFN.

-
- [1] A. A. Penzias and R. W. Wilson, *Astrophys. J.* **142** (1965) 419.
 - [2] R. K. Sachs and A. M. Wolfe, *Astrophys. J.* **147** (1967) 73 [*Gen. Rel. Grav.* **39** (2007) 1929].
 - [3] G. F. Smoot, C. L. Bennett, A. Kogut, E. L. Wright, J. Aymon, N. W. Boggess, E. S. Cheng and G. De Amici *et al.*, *Astrophys. J.* **396** (1992) L1.
 - [4] A. R. Liddle and D. H. Lyth, *Phys. Rept.* **231** (1993) 1 [[astro-ph/9303019](#)].
 - [5] J. E. Lidsey, A. R. Liddle, E. W. Kolb, E. J. Copeland, T. Barreiro and M. Abney, *Rev. Mod. Phys.* **69** (1997) 373 [[astro-ph/9508078](#)].
 - [6] P. S. Corasaniti, T. Giannantonio and A. Melchiorri, *Phys. Rev. D* **71** (2005) 123521 [[astro-ph/0504115](#)].
 - [7] P. Vielva, E. Martinez-Gonzalez and M. Tucci, *Mon. Not. Roy. Astron. Soc.* **365** (2006) 891 [[astro-ph/0408252](#)].
 - [8] J. D. McEwen, P. Vielva, M. P. Hobson, E. Martinez-Gonzalez and A. N. Lasenby, *Mon. Not. Roy. Astron. Soc.* **376**, 1211 (2007) [[astro-ph/0602398](#)].
 - [9] J. Lesgourgues, W. Valkenburg and E. Gaztanaga, *Phys. Rev. D* **77** (2008) 063505 [[arXiv:0710.5525](#) [astro-ph]].
 - [10] P. Zhang, *Phys. Rev. D* **73**, 123504 (2006) [[astro-ph/0511218](#)].
 - [11] S. Boughn and R. Crittenden, *Nature* **427** (2004) 45 [[astro-ph/0305001](#)].
 - [12] R. Scranton *et al.* [SDSS Collaboration], [[astro-ph/0307335](#)].
 - [13] P. Fosalba, E. Gaztanaga and F. Castander, *Astrophys. J.* **597** (2003) L89 [[astro-ph/0307249](#)].
 - [14] M. R. Nolta *et al.* [WMAP Collaboration], *Astrophys. J.* **608** (2004) 10 [[astro-ph/0305097](#)].
 - [15] N. Afshordi, Y. S. Loh and M. A. Strauss, *Phys. Rev. D* **69** (2004) 083524 [[astro-ph/0308260](#)].
 - [16] T. Giannantonio, R. G. Crittenden, R. C. Nichol, R. Scranton, G. T. Richards, A. D. Myers, R. J. Brunner and A. G. Gray *et al.*, *Phys. Rev. D* **74** (2006) 063520 [[astro-ph/0607572](#)].

- [17] A. Rassat, K. Land, O. Lahav and F. B. Abdalla, Mon. Not. Roy. Astron. Soc. **377** (2007) 1085 [[astro-ph/0610911](#)];
- [18] S. Ho, C. Hirata, N. Padmanabhan, U. Seljak and N. Bahcall, Phys. Rev. D **78** (2008) 043519 [[arXiv:0801.0642](#) [astro-ph]];
- [19] T. Giannantonio, R. Scranton, R. G. Crittenden, R. C. Nichol, S. P. Boughn, A. D. Myers and G. T. Richards, Phys. Rev. D **77** (2008) 123520 [[arXiv:0801.4380](#) [astro-ph]];
- [20] P. A. R. Ade *et al.* [Planck Collaboration], Astron. Astrophys. **571** (2014) A19 [[arXiv:1303.5079](#) [astro-ph.CO]].
- [21] P. A. R. Ade *et al.* [Planck Collaboration], [arXiv:1502.01595](#) [astro-ph.CO].
- [22] Z. Hou, R. Keisler, L. Knox, M. Millea and C. Reichardt, Phys. Rev. D **87** (2013) 083008 [[arXiv:1104.2333](#) [astro-ph.CO]].
- [23] We use the Newtonian gauge convention $g_{00} = -1 - 2\Phi$ and $g_{ij} = a^2\delta_{ij}(1 + 2\Phi)$.
- [24] R. Bowen, S. H. Hansen, A. Melchiorri, J. Silk and R. Trotta, Mon. Not. Roy. Astron. Soc. **334**, 760 (2002) [[astro-ph/0110636](#)].
- [25] At the present time the relevant length of photon trajectories is comparable to the horizon size, so that the main contribution to Eq. (1) comes from perturbations with $\lambda \sim \eta_0$ (the contributions of shorter wavelengths again average away). Therefore the late ISW effect influences only multipoles corresponding to $k \sim 1/\eta_0$, that is $\ell \sim 1$.
- [26] A. Manzotti and S. Dodelson, Phys. Rev. D **90**, no. 12, 123009 (2014) [[arXiv:1407.5623](#) [astro-ph.CO]].
- [27] P. S. Corasaniti, T. Giannantonio and A. Melchiorri, Phys. Rev. D **71**, 123521 (2005) [[astro-ph/0504115](#)].
- [28] A. Cabre, E. Gaztanaga, M. Manera, P. Fosalba and F. Castander, Mon. Not. Roy. Astron. Soc. **372**, L23 (2006) [[astro-ph/0603690](#)].
- [29] W. Hu and T. Okamoto, Astrophys. J. **574**, 566 (2002) [[astro-ph/0111606](#)].
- [30] D. M. Goldberg and D. N. Spergel, Phys. Rev. D **59**, 103002 (1999) [[astro-ph/9811251](#)].
- [31] B. Gold, Phys. Rev. D **71**, 063522 (2005) [[astro-ph/0411376](#)].
- [32] A. Lue, R. Scoccimarro and G. Starkman, Phys. Rev. D **69**, 044005 (2004) [[astro-ph/0307034](#)].
- [33] E. Di Valentino, A. Melchiorri, V. Salvatelli and A. Silvestri, Phys. Rev. D **86**, 063517 (2012) [[arXiv:1204.5352](#) [astro-ph.CO]].
- [34] <http://camb.info>.
- [35] A. Lewis, Phys. Rev. D **87**, no. 10, 103529 (2013) [[arXiv:1304.4473](#) [astro-ph.CO]].
- [36] A. Lewis and S. Bridle, Phys. Rev. D **66**, 103511 (2002) [[astro-ph/0205436](#)].
- [37] E. Calabrese, A. Slosar, A. Melchiorri, G. F. Smoot and O. Zahn, Phys. Rev. D **77**, 123531 (2008) [[arXiv:0803.2309](#) [astro-ph]].
- [38] D. J. Fixsen, Ap. J. **707**, 916-920 (2009)
- [39] N. Aghanim *et al.* [Planck Collaboration], [arXiv:1507.02704](#) [astro-ph.CO].
- [40] C. L. Bennett *et al.*, Ap. JS **208**, 20B (2013)
- [41] P. A. R. Ade *et al.* [Planck Collaboration], [arXiv:1502.01589](#) [astro-ph.CO].
- [42] P. A. R. Ade *et al.* [Planck Collaboration], [arXiv:1502.01591](#) [astro-ph.CO].
- [43] Z. Hou, R. Keisler, L. Knox, M. Millea and C. Reichardt, Phys. Rev. D **87**, 083008 (2013) [[arXiv:1104.2333](#) [astro-ph.CO]].
- [44] W. J. Percival *et al.* [SDSS Collaboration], Mon. Not. Roy. Astron. Soc. **401**, 2148 (2010) [[arXiv:0907.1660](#) [astro-ph.CO]].
- [45] F. Beutler, C. Blake, M. Colless, D. H. Jones, L. Staveley-Smith, L. Campbell, Q. Parker and W. Saunders *et al.*, Mon. Not. Roy. Astron. Soc. **416**, 3017 (2011) [[arXiv:1106.3366](#) [astro-ph.CO]].
- [46] C. Blake, E. Kazin, F. Beutler, T. Davis, D. Parkinson, S. Brough, M. Colless and C. Contreras *et al.*, Mon. Not. Roy. Astron. Soc. **418**, 1707 (2011) [[arXiv:1108.2635](#) [astro-ph.CO]].
- [47] N. Padmanabhan, X. Xu, D. J. Eisenstein, R. Scalzo, A. J. Cuesta, K. T. Mehta and E. Kazin, Mon. Not. Roy. Astron. Soc. **427**, no. 3, 2132 (2012) [[arXiv:1202.0090](#) [astro-ph.CO]].
- [48] L. Anderson, E. Aubourg, S. Bailey, D. Bizyaev, M. Blanton, A. S. Bolton, J. Brinkmann and J. R. Brownstein *et al.*, Mon. Not. Roy. Astron. Soc. **427**, no. 4, 3435 (2013) [[arXiv:1203.6594](#) [astro-ph.CO]].